

Original citation:

Wang, Manxin, Liu, Haitao, Huang, Tian and Chetwynd, D. G.. (2015) Compliance analysis of a 3-SPR parallel mechanism with consideration of gravity. Mechanism and Machine Theory, 84.

Permanent WRAP url:

<http://wrap.warwick.ac.uk/78035>

Copyright and reuse:

The Warwick Research Archive Portal (WRAP) makes this work by researchers of the University of Warwick available open access under the following conditions. Copyright © and all moral rights to the version of the paper presented here belong to the individual author(s) and/or other copyright owners. To the extent reasonable and practicable the material made available in WRAP has been checked for eligibility before being made available.

Copies of full items can be used for personal research or study, educational, or not-for-profit purposes without prior permission or charge. Provided that the authors, title and full bibliographic details are credited, a hyperlink and/or URL is given for the original metadata page and the content is not changed in any way.


Publisher's statement:

© 2015, Elsevier. Licensed under the Creative Commons Attribution-NonCommercial-NoDerivatives 4.0 International <http://creativecommons.org/licenses/by-nc-nd/4.0/>

A note on versions:

The version presented here may differ from the published version or, version of record, if you wish to cite this item you are advised to consult the publisher's version. Please see the 'permanent WRAP url' above for details on accessing the published version and note that access may require a subscription.

For more information, please contact the WRAP Team at: publications@warwick.ac.uk

warwick**publications**wrap

highlight your research

<http://wrap.warwick.ac.uk>

Compliance Analysis of a 3-SPR Parallel Mechanism with Consideration of Gravity

Manxin Wang ^a, Haitao Liu ^{a,b}, Tian Huang ^{a,c,*}, Derek G. Chetwynd ^c

^a Key Laboratory of Mechanism Theory and Equipment Design of Ministry of Education, Tianjin University, Tianjin 300072, China

^b Chair of Mechanics and Robotics, University of Duisburg-Essen, Duisburg 47057, Germany

^c School of Engineering, The University of Warwick, Coventry CV4 7AL, UK

Abstract:

By taking gravity and joint/link compliances into account, this paper presents a semi-analytical approach for compliance analysis of a 3-SPR parallel mechanism which forms the main body of a 5-DOF hybrid manipulator especially designed for high-speed machining and forced assembling in the aircraft industry. The approach is implemented in three steps: (1) kinetostatic analysis that considers both the externally applied wrench imposed upon the platform and the gravity of all moving components; (2) deflection analysis that takes into accounts of both joint and link compliances; (3) formulation of the component compliance matrices using a semi-analytical approach. The advantage of this approach is that the deflections of the platform caused by both the payload and gravity within the given task workspace can be evaluated in an effective manner. The computational results show that the deflection arising from gravity of the moving components may have significant influence on the pose accuracy of the end-effector.

Keyword: Compliance analysis, Gravitational effect, Parallel mechanism

1. Introduction

The existing category of five degrees of freedom (DOF) manipulators having hybrid architectures contains two families that are composed of a 3-DOF parallel mechanisms plus a 2-DOF rotating head attached to its platform. The first family essentially comprises those with a properly constrained active/passive limb plus a number of 6-DOF active limbs having six degrees of freedom [1, 2]. Here, an active limb is the limb having at least one actuated joint. A passive limb is the limb having no actuated joint. And the word ‘properly’ means that the type and number of DOF of the constrained limb are completely identical to those of the platform. Typical examples in this family are the well-known Tricept [3], George V [4] and TriVariant [5] among others [6]. Parallel mechanisms belonging to the second family are basically composed of three lower mobility limbs having 4 or 5 degrees of freedom. Typical example in this family is the Exechon robot [7]. These two families are especially designed for their applicability to light machining (such as deburring, drilling, cutting and welding), among other tasks, and they thereby have become of great interest to machine tool and aircraft builders in recent years.

Stiffness is one of the most important performance factors that should be considered for the above-mentioned 5-DOF hybrid manipulators when they are used for high-speed machining and/or forced assembling, for which high rigidity and high accuracy are crucial requirements. These requirements have led to enthusiastic and extensive investigations into stiffness modelling, evaluation and optimization. As far as the stiffness modelling is concerned the approaches available to hand can roughly be divided into two groups: numerical approaches by means of finite element analysis (FEA) or structure matrix analysis (SMA) [8-9]; and analytical or semi-analytical approaches [10-26] based upon the combination of fundamental robotic theory with FEA or structural mechanics. The FEA is the most accurate method because the complex 3D geometry of links, contact rigidity of joints, and distributed external forces (self-weight or gravity, for example) can be modelled precisely. However, very high computational costs arise as the FE models have to be re-meshed over and over again with the changing configurations. Consequently, comprehensive analytical/semi-analytical modelling approaches are required in order to allow stiffness evaluation to be carried out throughout the entire workspace in an effective manner either in the preliminary or in the final design stage.

Analytical/semi-analytical stiffness modelling of parallel mechanisms can be traced back to the work of Gosselin [10] in which merely the actuator compliances were taken into account. By taking into account the component compliances in terms of tension/compression, bending and torsion, a plenty of work was carried out by Zhang and Gosselin [11-13] for the stiffness analyses of Tricept robots. They also proposed the elegant concept of the ‘virtual joint’ to formulate the bending compliance of a properly constrained passive limb within the Tricept and its variants, resulting in a simplified bending stiffness model represented by three lumped springs. Recently, the concept of ‘virtual joint’ was significantly extended by Pashkevich *et al* [14-16], resulting in a multidimensional lumped-parameter model formulated in terms of localized 6-DOF virtual springs for describing the link/joint compliances. The model formulated in this way is a direct map from the rigidity of links/joints to the stiffness of the end-effector.

By dividing the link/joint compliances into two groups associated respectively with actuations and constraints, screw theory based approach may serve as a useful tool for analytical/semi-analytical stiffness modelling of lower mobility parallel mechanisms. The initiative along this track was taken by Joshi and Tsai [27] in formulating the overall Jacobian.

* Corresponding author. Tel./fax: +86 2227405280.

E-mail addresses: tianhuang@tju.edu.cn, th@eng.warwick.ac.uk (T. Huang)

The idea was then extended by Huang and colleagues [28] into the generalized Jacobian. The difference is that the generalized Jacobian considers the theoretically inaccessible instantaneous motions between the joint space and operation space, which is an important issue in the stiffness and accuracy analysis. Based upon the overall and generalized Jacobians, the stiffness analyses of a number of lower mobility parallel manipulators have been investigated [17-26]. The advantages of the screw theory based approach is that it enables the Cartesian stiffness matrix to be decomposed into two meaningful components associated respectively with actuations and constraints, providing designers with clear and useful guidelines for taking appropriate measures to improve static performance of the system.

It should be pointed out that besides the deflections caused by the payload exerted upon the end-effector, the deflections caused by the gravity of the robot structure itself should be considered in the compliance analysis of the 5-DOF hybrid manipulators, particularly for applications that orient them primarily horizontally. Several attempts have been made to deal with this problem by treating gravity as a concentrated force[29-31], or as equivalent pairs of parallel forces applied on the adjacent joints[16]. However, these treatments are insufficient in the cases where the link compliances are not negligible, thus remaining an open issue to be investigated.

This paper presents a semi-analytical approach for compliance analysis, applied explicitly to a 3-SPR parallel mechanism which forms the main body of a 5-DOF hybrid manipulator especially designed for high-speed machining and forced assembling. Having outlined the existing challenges above, the paper is organized as follows. The system description and inverse displacement analysis are addressed briefly in Section 2. Section 3 then executes the detailed procedure for deflection analysis of the mechanism, concentrating upon: (1) formulation of a linear map between joint forces and an externally equivalent applied wrench imposed on the platform; (2) establishment of a precise model for the joint deflections; and (3) formulation of the component compliance matrices in the joint space using a semi-analytical approach. A numerical example is given in Section 4 to illustrate the effectiveness of the approach and conclusions are drawn in Section 5.

2. System Description and Inverse Kinematics

Fig.1 shows a 3D view of the 5-DOF hybrid manipulator under consideration, which is essentially composed of a 3-SPR parallel mechanism plus a 2-DOF rotating head attached to the platform *via* a trust bearing. The parallel mechanism consists of a platform, a base, and three identical SPR limbs. The major distinctions between the current design and the Exechon robot [7] are: 1) the use of three identical SPR limbs instead of two UPR plus one SPR limbs, 2) the use of fork type joints to reduce the base size, and 3) the use of cants with inclination angles to the base to reduce the overhang distance of the centre of the spherical joints and thus avoid interference between the base and limbs. The spherical joint contains a rotating fork, a rotating block and a carriage, they are sequentially connected by shafts and bearings. In order to achieve a compact design, the rotating block is embedded within the rotating fork and carriage. The lead-screw is then placed through the rotating block and the carriage.

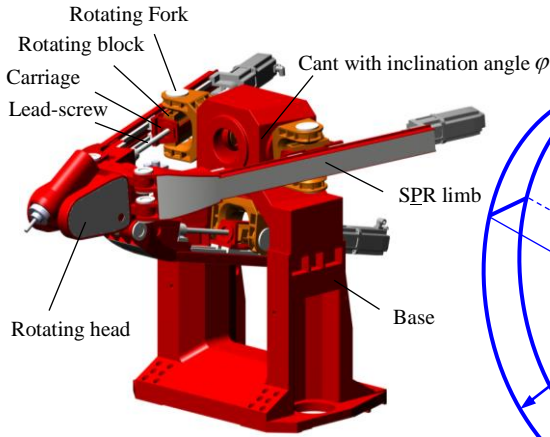


Fig.1 3D model of the 3-SPR parallel mechanism plus a 2-DOF rotating head

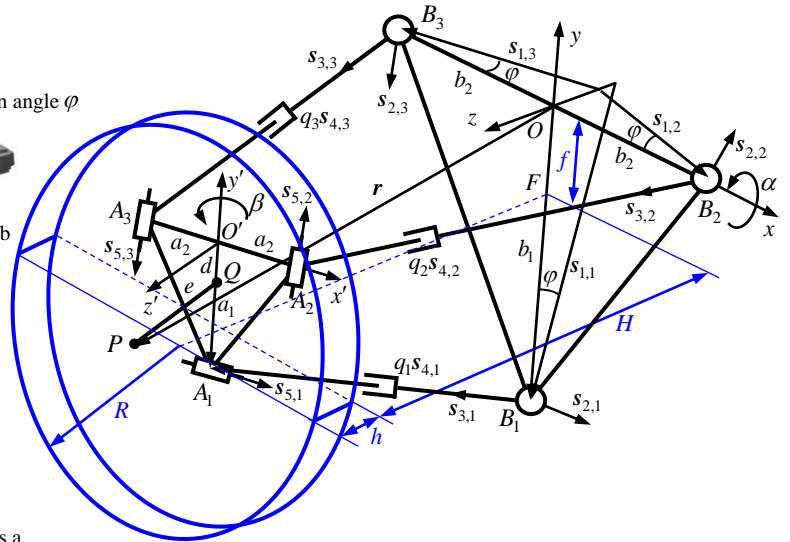


Fig.2 Schematic diagram of a 3-SPR parallel mechanism

Fig.2 shows the schematic diagram of the 3-SPR parallel mechanism. Let B_i be the centre of the S joint connecting the i th limb with the base, forming an isosceles triangle $\Delta B_1 B_2 B_3$, and let A_i be the centre of the R joint connecting the limb with the platform, forming an isosceles triangle $\Delta A_1 A_2 A_3$. Then, place a reference frame $\{R\}$ attached to the base with O being located at the centre of $\overline{B_2 B_3}$ such that $z \perp \Delta B_1 B_2 B_3$ and $y \perp \overline{B_2 B_3}$. Meanwhile, place a body fixed frame $\{R'\}$ attached to the platform with O' being located at the centre of $\overline{A_2 A_3}$ such that $z' \perp \Delta A_1 A_2 A_3$ and

$y' \perp \overline{A_2 A_3}$. For convenience of defining the link/joint compliances within a limb, place a set of body fixed frames $\{R_{j,i}\}$ attached to one of two elements of the j th joint in the i th limb with $s_{j,i}$ being the unit vector of the joint axis. For this particular problem, $\{R_{j,i}\}$ is sequentially attached to the axis of the j th ($j=1,2,3$) revolute joint within the spherical joint, $\{R_{4,i}\}$ is attached to the carriage with B_i being its origin, and $\{R_{5,i}\}$ is attached to the limb body with A_i being its origin. Fig.3 and 4 show the locations of the axes of these frames.

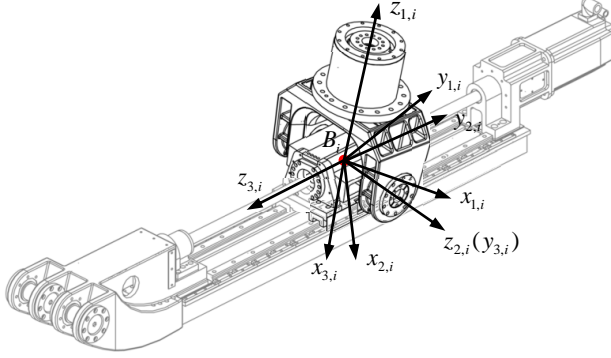


Fig.3 Body fixed frames of the S joint within the i th limb

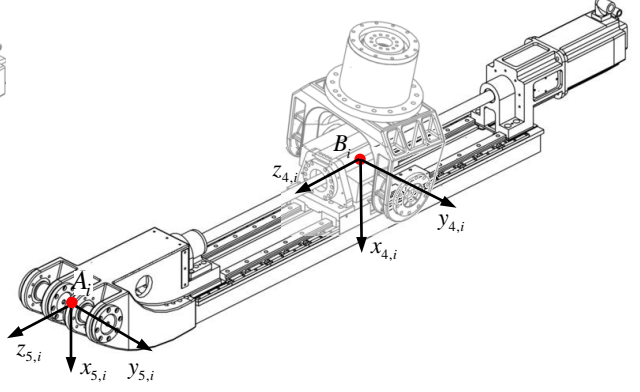


Fig.4 Body fixed frames of the i th limb-body assembly

According to the frame settings described above, the joint axes are arranged in the ways

$$\begin{aligned} s_{1,i} \perp s_{2,i}, s_{2,i} \perp s_{3,i}, s_{3,i} // s_{4,i}, s_{4,i} \perp s_{5,i}, i=1,2,3 \\ s_{5,2} // s_{5,3}, s_{5,1} \perp s_{5,2}, s_{5,2} \perp \overline{A_2 A_3} \end{aligned} \quad (1)$$

such that B_2, B_3, A_3, A_2 are forced to be coplanar. Then, the orientation matrix \mathbf{R} of $\{R'\}$ with respect to $\{R\}$ can be expressed in terms of two Cardan angles, i.e. α about the x axis and β about the y' axis, as

$$\mathbf{R} = \text{Rot}(x, \alpha) \text{Rot}(y', \beta) = \begin{bmatrix} \cos \beta & 0 & \sin \beta \\ \sin \alpha \sin \beta & \cos \alpha & -\sin \alpha \cos \beta \\ -\cos \alpha \sin \beta & \sin \alpha & \cos \alpha \cos \beta \end{bmatrix} = [\mathbf{u} \quad \mathbf{v} \quad \mathbf{w}] \quad (2)$$

where \mathbf{u} , \mathbf{v} and \mathbf{w} are the unit vectors of the three orthogonal axes of $\{R'\}$.

Given the dimensional parameters and the position of the point P , an inverse displacement analysis is carried out as the prerequisite for deflection analysis of the 3-SPR parallel mechanism. As shown in Fig.2, the position vector, $\mathbf{r} = (x \quad y \quad z)^T$, of the point P can be expressed by

$$\mathbf{r} = \mathbf{b}_i + q_i \mathbf{s}_{4,i} - \mathbf{c}_i, \quad \mathbf{c}_i = \mathbf{a}_i + d\mathbf{v} - e\mathbf{w} \quad (3)$$

where q_i is the length of the i th limb; \mathbf{b}_i and \mathbf{a}_i are the position vectors pointing from O to B_i , and from O' to A_i , respectively. Also,

$$\begin{aligned} \mathbf{a}_i &= \mathbf{R} \mathbf{a}_{0i}, \quad \mathbf{a}_{0i} = a_i \mathbf{s}_i, \quad \mathbf{b}_i = b_i \mathbf{s}_i, \quad \mathbf{s}_i = (\cos \gamma_i \quad \sin \gamma_i \quad 0)^T \\ a_1 &= \overline{O'A_1}, \quad a_2 = a_3 = \overline{O'A_2} = \overline{O'A_3}, \quad b_1 = \overline{OB_1}, \quad b_2 = b_3 = \overline{OB_2} = \overline{OB_3} \\ d &= \overline{O'Q}, \quad e = \overline{PQ}, \quad \gamma_1 = -\pi/2, \quad \gamma_2 = 0, \quad \gamma_3 = \pi \end{aligned} \quad (4)$$

Note that the geometric constraint $s_{5,2} // s_{5,3}$ given in Eq.(1) restricts OO' to be lying in the plane $B_2 B_3 A_3 A_2$ normal to \mathbf{v} . This consideration leads to

$$\mathbf{v}^T \mathbf{r} + d = 0 \quad (5)$$

Also, note that $s_{5,1} \perp s_{4,1}$ and $s_{5,1} \perp \mathbf{c}_1$ such that

$$\mathbf{u}^T (\mathbf{r} - \mathbf{b}_1) = 0 \quad (6)$$

Solving Eq.(5) and (6) yields

$$\alpha = \begin{cases} 2 \arctan \frac{z - \sqrt{y^2 + z^2 - d^2}}{y - d} & y \neq d \\ -2 \arctan \frac{d}{z} & y = d \end{cases}, \quad \beta = \arctan \left(\frac{x}{z \cos \alpha - (y + b_1) \sin \alpha} \right) \quad (7)$$

Then, \mathbf{R} can be determined using Eq.(2) and the inverse displacement problem can be solved by

$$q_i = |\mathbf{r} - \mathbf{b}_i + \mathbf{c}_i|, \quad \mathbf{s}_{4,i} = (\mathbf{r} - \mathbf{b}_i + \mathbf{c}_i) / q_i, \quad \mathbf{s}_{3,i} = \mathbf{s}_{4,i} \\ \mathbf{s}_{5,1} = \mathbf{u}, \quad \mathbf{s}_{5,2} = \mathbf{v}, \quad \mathbf{s}_{5,3} = -\mathbf{v}, \quad \mathbf{s}_{1,i} = (\cos \varphi \cos \gamma_i \quad \cos \varphi \sin \gamma_i \quad \sin \varphi)^T, \quad \mathbf{s}_{2,i} = \frac{\mathbf{s}_{3,i} \times \mathbf{s}_{1,i}}{|\mathbf{s}_{3,i} \times \mathbf{s}_{1,i}|} \quad i = 1, 2, \quad (8)$$

where φ is the inclination angle of the cant in the base.

3. Compliance Analysis

This section introduces a semi-analytic compliance model of the 3-SPR parallel mechanism that simultaneously takes into account all significant component compliances, including axial and bending compliances of the links, and compliances of the S, P and R joints. By assuming the system is linearly elastic in nature, we treat the base and platform (including the 2-DOF rotating head) as rigid bodies since superposition can be used wherever required to consider their compliances. This analysis also takes into account the deflections induced by gravity of all the movable components.

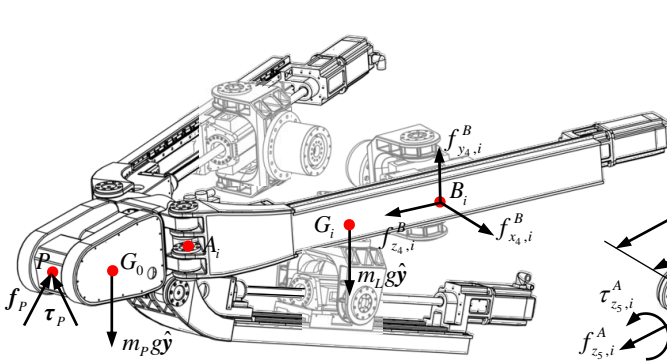


Fig.5 Free body diagram of the parallel mechanism

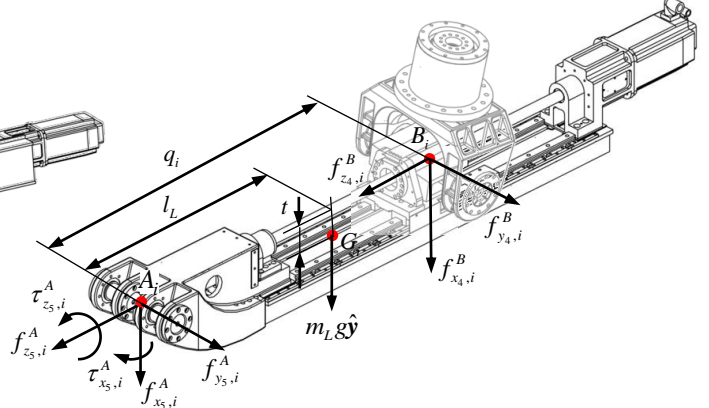


Fig.6 Free body diagram of the *i*th limb-body assembly

3.1 Force Analysis

Force analysis of the 3-SPR parallel mechanism is concerned with the formulation of a linear map between the externally applied wrench imposed upon the platform and the reaction forces at B_i as shown in Fig.5. By considering all forces and by taking the moment of all forces about P , the static equilibrium equations can be expressed as

$$\mathbf{f}_p - m_p \mathbf{g} \hat{\mathbf{y}} - 3m_L \mathbf{g} \hat{\mathbf{y}} = \sum_{i=1}^3 (\mathbf{f}_{x4,i}^B \mathbf{n}_i + \mathbf{f}_{y4,i}^B \mathbf{s}_{5,i} + \mathbf{f}_{z4,i}^B \mathbf{s}_{4,i}) \\ \tau_p - m_p g \mathbf{R}(\mathbf{r}_{G_0} - \mathbf{r}_{P_0}) \times \hat{\mathbf{y}} - m_L g (\mathbf{c}_i - (l_L \mathbf{s}_{4,i} - \mathbf{m}_i)) \times \hat{\mathbf{y}} = \sum_{i=1}^3 (\mathbf{f}_{x4,i}^B (\mathbf{c}_i - q_i \mathbf{s}_{4,i}) \times \mathbf{n}_i + \mathbf{f}_{y4,i}^B (\mathbf{c}_i - q_i \mathbf{s}_{4,i}) \times \mathbf{s}_{5,i} + \mathbf{f}_{z4,i}^B \mathbf{c}_i \times \mathbf{s}_{4,i}) \\ \mathbf{n}_i = \mathbf{s}_{5,i} \times \mathbf{s}_{4,i}, \quad \hat{\mathbf{y}} = (0 \quad 1 \quad 0)^T \quad (9)$$

where \mathbf{f}_p and τ_p are the externally applied force and moment imposed upon the platform at P ; m_p is the mass and \mathbf{r}_{G_0} is the position vector of the mass centre G_0 of the platform evaluated in $\{R'\}$; $\mathbf{r}_{P_0} = (0 \quad -d \quad e)^T$; m_L is the mass and $l_L(t)$ is the projection of the distance from the mass centre G_i of the limb-body assembly onto A_i along $\mathbf{s}_{4,i}(\mathbf{n}_i)$; $\hat{\mathbf{y}}$ is placed in the direction opposite to the gravitational field; $\mathbf{f}_{x4,i}^B$, $\mathbf{f}_{y4,i}^B$ and $\mathbf{f}_{z4,i}^B$ are the reaction forces along the $x_{4,i}$, $y_{4,i}$, $z_{4,i}$ axes at B_i . These reaction forces cannot be solved directly because there are nine unknowns in the six equilibrium equations. Consider, however, the free-body diagram of the *i*th limb-body assembly as shown in Fig.6, which exposes the reaction forces and couples in the revolute joint. Then, taking moments of all

forces about A_i gives

$$\tau_{x_5,i}^A \mathbf{n}_i + \tau_{z_5,i}^A \mathbf{s}_{4,i} - (l_L \mathbf{s}_{4,i} - t \mathbf{n}_i) \times (-m_L g \hat{\mathbf{y}}) = -q_i \mathbf{s}_{4,i} \times (f_{x_4,i}^B \mathbf{n}_i + f_{y_4,i}^B \mathbf{s}_{5,i}), \quad i=1,2,3 \quad (10)$$

where $\tau_{x_5,i}^A$ and $\tau_{z_5,i}^A$ denote the reaction couples about the $x_{5,i}$ and $z_{5,i}$ axes respectively. Now, taking the dot product on both sides of Eq.(10) with $\mathbf{s}_{5,i}$ yields

$$f_{x_4,i}^B = -\frac{m_L g}{q_i} (t \mathbf{s}_{4,i} + l_L \mathbf{n}_i)^T \hat{\mathbf{y}}, \quad i=1,2,3 \quad (11)$$

Substituting Eq.(11) into Eq.(9) and rewriting in matrix form results in

$$\mathbf{\$}_w = \mathbf{J}^T \boldsymbol{\rho}_w \quad (12)$$

where

$$\begin{aligned} \mathbf{\$}_w &= \mathbf{\$}_{w,E} + \mathbf{\$}_{w,G_p} + \mathbf{\$}_{w,G_L}, \quad \mathbf{\$}_{w,E} = \begin{pmatrix} f_p \\ \tau_p \end{pmatrix}, \quad \mathbf{\$}_{w,G_p} = -m_p g \begin{pmatrix} \hat{\mathbf{y}} \\ \mathbf{R}(\mathbf{r}_{G_0} - \mathbf{r}_{P_0}) \times \hat{\mathbf{y}} \end{pmatrix} \\ \mathbf{\$}_{w,G_L} &= -m_L g \sum_{i=1}^3 \left(\begin{pmatrix} \hat{\mathbf{y}} \\ (\mathbf{c}_i - l_L \mathbf{s}_{4,i} + t \mathbf{n}_i) \times \hat{\mathbf{y}} \end{pmatrix} - \frac{l_L}{q_i} \begin{pmatrix} \mathbf{n}_i \\ (\mathbf{c}_i - q_i \mathbf{s}_{4,i}) \times \mathbf{n}_i \end{pmatrix} \mathbf{n}_i^T \hat{\mathbf{y}} - \frac{t}{q_i} \begin{pmatrix} \mathbf{n}_i \\ (\mathbf{c}_i - q_i \mathbf{s}_{4,i}) \times \mathbf{n}_i \end{pmatrix} \mathbf{s}_{4,i}^T \hat{\mathbf{y}} \right) \end{aligned}$$

$\mathbf{\$}_w$ is the resultant externally applied wrench imposed at P with $\mathbf{\$}_{w,G_p}$ and $\mathbf{\$}_{w,G_L}$ being the components produced by the gravity of the platform and limb-body assemblies, respectively; and

$$\begin{aligned} \mathbf{J} &= [\mathbf{J}_a^T \quad \mathbf{J}_c^T]^T, \quad \mathbf{J}_a = \begin{bmatrix} \mathbf{s}_{4,1} & \mathbf{s}_{4,2} & \mathbf{s}_{4,3} \\ \mathbf{c}_1 \times \mathbf{s}_{4,1} & \mathbf{c}_2 \times \mathbf{s}_{4,2} & \mathbf{c}_3 \times \mathbf{s}_{4,3} \end{bmatrix}^T, \quad \mathbf{J}_c = \begin{bmatrix} \mathbf{s}_{5,1} & \mathbf{s}_{5,2} & \mathbf{s}_{5,3} \\ (\mathbf{c}_1 - q_1 \mathbf{s}_{4,1}) \times \mathbf{s}_{5,1} & (\mathbf{c}_2 - q_2 \mathbf{s}_{4,2}) \times \mathbf{s}_{5,2} & (\mathbf{c}_3 - q_3 \mathbf{s}_{4,3}) \times \mathbf{s}_{5,3} \end{bmatrix}^T \\ \boldsymbol{\rho}_w &= (\boldsymbol{\rho}_{wa}^T \quad \boldsymbol{\rho}_{wc}^T)^T, \quad \boldsymbol{\rho}_{wa} = (\rho_{wa,1} \quad \rho_{wa,2} \quad \rho_{wa,3})^T, \quad \rho_{wa,i} = f_{z_4,i}^B, \quad \boldsymbol{\rho}_{wc} = (\rho_{wc,1} \quad \rho_{wc,2} \quad \rho_{wc,3})^T, \quad \rho_{wc,i} = f_{y_4,i}^B \end{aligned}$$

\mathbf{J} is the overall or generalized Jacobian [27, 28] with \mathbf{J}_a and \mathbf{J}_c being the components associated respectively with actuations and constraints; and $\boldsymbol{\rho}_w$ is the joint force vector with $\boldsymbol{\rho}_{wa}$ and $\boldsymbol{\rho}_{wc}$ being those corresponding to \mathbf{J}_a and \mathbf{J}_c . Since each row of \mathbf{J}_a (\mathbf{J}_c) represents a unit wrench, Eq.(12) can be interpreted physically as meaning that the externally applied wrench imposed upon the platform must be equilibrated by all wrenches of actuations and constraints imposed by all limbs.

3.2 Deflection Analysis

Deflection analysis of the 3-SPR parallel mechanism is concerned with the formulation of the linear map between deflection twist of the platform and the virtual linear deflections at B_i . Utilizing the reciprocal theorem in elastic mechanics, readily proves the relationship that

$$\delta \mathbf{r} + \delta \boldsymbol{\alpha} \times (\mathbf{c}_i - q_i \mathbf{s}_{4,i}) = \delta_{x_4,i}^B \mathbf{n}_i + \delta_{y_4,i}^B \mathbf{s}_{5,i} + \delta_{z_4,i}^B \mathbf{s}_{4,i}, \quad i=1,2,3 \quad (13)$$

where $\delta \mathbf{r}$ and $\delta \boldsymbol{\alpha}$ are the linear deflection at P and the angular deflection of the platform; and $\delta_{x_4,i}^B$, $\delta_{y_4,i}^B$ and $\delta_{z_4,i}^B$ are the virtual infinitesimal displacements at B_i along the $x_{4,i}$, $y_{4,i}$ and $z_{4,i}$ axes when the joint constraints at B_i are assumed to be released to free the elastic deformation energy stored in the system.

Taking dot products on both sides of Eq.(13) with $\mathbf{s}_{4,i}$ and $\mathbf{s}_{5,i}$ respectively yields

$$\begin{aligned} \mathbf{s}_{4,i}^T \delta \mathbf{r} + (\mathbf{c}_i \times \mathbf{s}_{4,i})^T \delta \boldsymbol{\alpha} &= \delta_{z_4,i}^B, \\ \mathbf{s}_{5,i}^T \delta \mathbf{r} + ((\mathbf{c}_i - q_i \mathbf{s}_{4,i}) \times \mathbf{s}_{5,i})^T \delta \boldsymbol{\alpha} &= \delta_{y_4,i}^B, \end{aligned} \quad i=1,2,3 \quad (14)$$

Rewriting Eq.(14) in matrix form finally results in

$$\begin{aligned} \mathbf{J} \mathbf{\$}_t &= \boldsymbol{\rho}_t \\ \mathbf{\$}_t &= (\delta \mathbf{r}^T \quad \delta \boldsymbol{\alpha}^T)^T, \quad \boldsymbol{\rho}_t = (\boldsymbol{\rho}_{ta}^T \quad \boldsymbol{\rho}_{tc}^T)^T \\ \boldsymbol{\rho}_{ta} &= (\rho_{ta,1} \quad \rho_{ta,2} \quad \rho_{ta,3})^T, \quad \rho_{ta,i} = \delta_{z_4,i}^B, \quad \boldsymbol{\rho}_{tc} = (\rho_{tc,1} \quad \rho_{tc,2} \quad \rho_{tc,3})^T, \quad \rho_{tc,i} = \delta_{y_4,i}^B \end{aligned} \quad (15)$$

where $\$t$ represents the deflection twist of the platform at P ; ρ_t denotes the joint deflection vector with ρ_{ta} and ρ_{tc} being those associated with J_a and J_c . Note that ρ_{ta} and ρ_{tc} should be further decomposed into two components, i.e.

$$\rho_{ta} = \rho'_{ta} + \rho''_{ta}, \quad \rho'_{ta} = (\rho'_{ta,1} \quad \rho'_{ta,2} \quad \rho'_{ta,3})^T, \quad \rho''_{ta} = (\rho''_{ta,1} \quad \rho''_{ta,2} \quad \rho''_{ta,3})^T \quad (16)$$

$$\rho_{tc} = \rho'_{tc} + \rho''_{tc}, \quad \rho'_{tc} = (\rho'_{tc,1} \quad \rho'_{tc,2} \quad \rho'_{tc,3})^T, \quad \rho''_{tc} = (\rho''_{tc,1} \quad \rho''_{tc,2} \quad \rho''_{tc,3})^T \quad (17)$$

where $\rho'_{ta,i}$ ($\rho'_{tc,i}$) is caused by the compliance of the i th limb under the action of the force $\rho_{wa,i}$ ($\rho_{wc,i}$), and $\rho''_{ta,i}$ ($\rho''_{tc,i}$) is caused by the compliance of the i th limb under the action of the distributed gravity of the limb itself. The procedure to evaluate $\rho''_{ta,i}$ and $\rho''_{tc,i}$ will be addressed in Section 3.5

3.3 Compliance Modelling

Having developed the two linear maps above, the deflection model of the mechanism is easily obtained. Assuming each individual component is linearly elastic, Hooke's law gives

$$\rho'_{ta,i} = c_{aa,i} \rho_{wa,i} + c_{ac,i} \rho_{wc,i}, \quad \rho'_{tc,i} = c_{cc,i} \rho_{wc,i} + c_{ca,i} \rho_{wa,i}, \quad i = 1, 2, 3 \quad (18)$$

where $c_{aa,i}$ ($c_{cc,i}$) can be interpreted physically as the deflection along the $z_{4,i}$ ($y_{4,i}$) axis produced by a unit joint force $\rho_{wa,i}$ ($\rho_{wc,i}$) in the i th limb; $c_{ac,i}$ ($c_{ca,i}$) denotes the coupled deflection along the $z_{4,i}$ ($y_{4,i}$) axis produced by a unit joint force $\rho_{wc,i}$ ($\rho_{wa,i}$); And $c_{ac,i} = c_{ca,i}$ because the system is assumed elastic linear in nature. Note that $c_{aa,i}$, $c_{cc,i}$ and $c_{ac,i}$ (or $c_{ca,i}$) are usually not constants but configuration dependent. Rewriting Eq.(18) in matrix form results in

$$\begin{aligned} \rho'_{ta} &= \bar{C}_{aa} \rho_{wa} + \bar{C}_{ac} \rho_{wc}, \quad \rho'_{tc} = \bar{C}_{cc} \rho_{wc} + \bar{C}_{ac} \rho_{wa} \\ \bar{C}_{aa} &= \begin{bmatrix} c_{aa,1} & & \\ & c_{aa,2} & \\ & & c_{aa,3} \end{bmatrix}, \quad \bar{C}_{cc} = \begin{bmatrix} c_{cc,1} & & \\ & c_{cc,2} & \\ & & c_{cc,3} \end{bmatrix}, \quad \bar{C}_{ac} = \begin{bmatrix} c_{ac,1} & & \\ & c_{ac,2} & \\ & & c_{ac,3} \end{bmatrix} \end{aligned} \quad (19)$$

where \bar{C}_{aa} (\bar{C}_{cc}) is referred to as the compliance matrix of actuations (constraints) in the joint space. \bar{C}_{ac} denotes the coupled compliance matrix between the directions of actuations and constraints. Substituting Eqs.(12) and (19) into Eq.(15) and assuming J is non-singular [32] finally results in the deflection model of the 3-SPR parallel mechanism which accounts for the gravity of the platform and limb-body assemblies. Thus,

$$\$t = C \$w + J^{-1} \rho''_t, \quad C = (J^T \bar{C}^{-1} J)^{-1}, \quad \bar{C} = \begin{bmatrix} \bar{C}_{aa} & \bar{C}_{ac} \\ \bar{C}_{ac}^T & \bar{C}_{cc} \end{bmatrix}, \quad \rho''_t = (\rho''_{ta}^T \quad \rho''_{tc}^T)^T \quad (20)$$

where C is referred to as the compliance matrix in the Cartesian space. It is easy to see that model developed here contains two components, i.e., the deflection caused by resultant externally applied wrench imposed upon the platform and that caused by the deflections ρ''_t arising from the distributed gravity of the limb-body assemblies. Obviously, $\$t$ in Eq.(20) can also be decomposed into another two components, i.e.,

$$\$t = \$t_{t,E} + \$t_{t,G} \quad (21)$$

where $\$t_{t,E} = C \$w_{t,E}$ is the deflection twist of the platform caused by the externally applied wrench $\$w_{t,E}$ imposed upon the platform, leading to a conventional compliance model neglecting gravity; and $\$t_{t,G}$ is that caused by the gravity of the movable components. Of course, further decomposition can also be made on $\$t_{t,G}$ such that

$$\$t_{t,G} = \$t_{t,G_p} + \$t_{t,G_L}, \quad \$t_{t,G_p} = C \$w_{w,G_p}, \quad \$t_{t,G_L} = C \$w_{w,G_L} + J^{-1} \rho''_t \quad (22)$$

where $\$t_{t,G_p}$ and $\$t_{t,G_L}$ are the deflection twists associated respectively with the gravity of the platform and limb-body assemblies. For simplicity, the two components $C \$w_{w,G_L}$ and $J^{-1} \rho''_t$ in $\$t_{t,G_L}$ are hereinafter denoted by $\$'_{t,G_L}$ and $\$''_{t,G_L}$ respectively.

3.4 Formulation of \bar{C}_{aa} , \bar{C}_{cc} and \bar{C}_{ac}

For simplicity, we temporarily omit the subscript ‘ i ’ during this evaluation of the elements in \bar{C}_{aa} , \bar{C}_{cc} and \bar{C}_{ac} ; the process applies equally to each limb. For a general link/joint, the compliance matrix should be symmetrical and have off-diagonal elements **by considering the coupled deflections between different directions. Then** the compliance matrix of a link/joint evaluated in $\{R_j\}$ with respect to its origin D can be formulated as

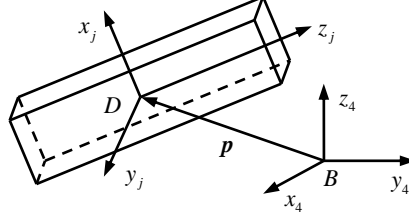


Fig.7 A link model for compliance evaluation and transformation

$$C_j^D = \begin{bmatrix} C_{j,t}^D & (C_{j,tr}^D)^T \\ C_{j,tr}^D & C_{j,r}^D \end{bmatrix} \quad (23)$$

where $C_{j,t}^D$ ($C_{j,r}^D$) denotes the linear (angular) compliance matrix, $C_{j,tr}^D$ denotes the coupled matrix between the linear and angular compliance. The linear compliance matrix expressed in our limb reference frame $\{R_4\}$ then follows the well-known compliance (or stiffness) transformation (see Fig.7), typically derived by the principle of virtual work. This consideration gives

$$C_{4,t}^B = R_{4j} C_{j,t}^D R_{4j}^T - \tilde{p} R_{4j} C_{j,r}^D R_{4j}^T \tilde{p} + \tilde{p} R_{4j} C_{j,tr}^D R_{4j}^T + (\tilde{p} R_{4j} C_{j,tr}^D R_{4j}^T)^T \quad (24)$$

where $R_{4j} = [\mathbf{u}_{4j} \ \mathbf{v}_{4j} \ \mathbf{w}_{4j}]$ denotes the orientation matrix of $\{R_j\}$ with respect to $\{R_4\}$, and \tilde{p} denotes the skew matrix of the vector \mathbf{p} pointing from B to D as shown in Fig.7. In this particular problem, the point D is either the centre of the spherical joint B or the centre of the revolute joint A ; \mathbf{p} has zero length in the former case, while the relative orientation is the same for the both.

At the same time, since only the directions of actuations and constraints are taken into account, the compliance matrix of the same link/joint evaluated in $\{R_4\}$ with respect to B can be modelled as

$$C_{4,t}^B = \begin{bmatrix} \infty & & \\ & c_{y_4 y_4}^B & c_{z_4 y_4}^B \\ & \text{sym} & c_{z_4 z_4}^B \end{bmatrix} \quad (25)$$

Note that “ ∞ ” means the compliance coefficient along the x_4 axis is infinite, meaning that the virtual displacement along the x_4 axis is a rigid body motion for fulfilling the compatibility conditions as all limbs share the same platform. $c_{y_4 y_4}^B$, $c_{z_4 z_4}^B$ and $c_{y_4 z_4}^B$ (or $c_{z_4 y_4}^B$) denote the linear rigidities in the directions of actuations (z_4), constraints (y_4) and the coupling between them, respectively.

To evaluate the component compliances, we group all the parts within an SPR limb into one of two sub-assemblies. Referring to Fig.8, the first sub-assembly comprises the R joint and the limb body, whereas the second sub-assembly comprises the prismatic joint (including the lead-screw assembly with its supporting bearings and the motor) and the spherical joint. The elements in \bar{C}_{aa} , \bar{C}_{cc} and \bar{C}_{ac} can then be modelled by

$$c_{aa} = \sum_{k=1}^2 c_{z_4 z_4, k}^B, \quad c_{cc} = \sum_{k=1}^2 c_{y_4 y_4, k}^B, \quad c_{ac} = \sum_{k=1}^2 c_{y_4 z_4, k}^B \quad (26)$$

where $c_{y_4 y_4, k}^B$ ($c_{z_4 z_4, k}^B$) denotes the linear compliance coefficient of the k th sub-assembly evaluated at B along the y_4 (z_4) axis. $c_{y_4 z_4, k}^B$ denotes the corresponding coupled compliance coefficient between the two directions.

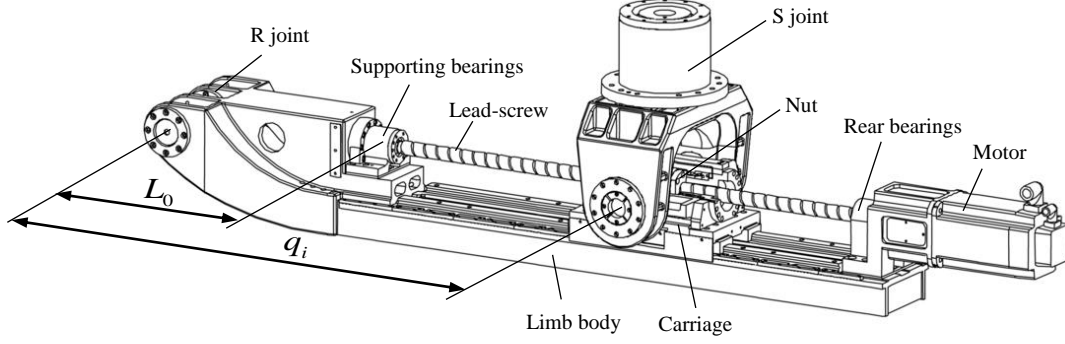


Fig.8 A limb model for compliance evaluation

(z_4) axis. $c_{y_4 z_4, k}^B$ denotes the corresponding coupled compliance coefficient between the two directions.

For the first sub-assembly, expansion of Eq.(24) yields

$$c_{y_4 y_4, 1}^B = c_{y_4 y_4, L_body}^B + c_{y_5 y_5, R_joint}^A + q^2 c_{x_5 \alpha_5, R_joint}^A, \quad c_{z_4 z_4, 1}^B = c_{z_4 z_4, L_body}^B + c_{z_5 z_5, R_joint}^A, \quad c_{y_4 z_4, 1}^B = c_{y_4 z_4, L_body}^B \quad (27)$$

where $c_{y_4 y_4, L_body}^B$ and $c_{z_4 z_4, L_body}^B$ are the linear compliance coefficients of the limb-body evaluated at B along the y_4 and z_4 axes; $c_{y_5 y_5, R_joint}^A$ and $c_{z_5 z_5, R_joint}^A$ ($c_{x_5 \alpha_5, R_joint}^A$) denote the linear (angular) compliance coefficients of the revolute joint evaluated at A along the y_5 and z_5 axes (about the x_5 axis); $c_{y_4 z_4, L_body}^B$ is the coupled compliance coefficient of the limb-body between the y_4 and z_4 axes. Note that $c_{y_5 y_5, R_joint}^A$, $c_{z_5 z_5, R_joint}^A$ and $c_{x_5 \alpha_5, R_joint}^A$ are constants while the others are functions of the limb length.

Similarly, expansion of Eq.(24) for the second sub-assembly leads to the following expressions

$$c_{y_4 y_4, 2}^B = c_{y_4 y_4, S_joint}^B + c_{y_4 y_4, P_joint}^B, \quad c_{z_4 z_4, 2}^B = c_{z_4 z_4, S_joint}^B + c_{z_4 z_4, P_joint}^B, \quad c_{y_4 z_4, 2}^B = c_{y_4 z_4, S_joint}^B \quad (28)$$

where $c_{y_4 y_4, S_joint}^B$ ($c_{y_4 y_4, P_joint}^B$) and $c_{z_4 z_4, S_joint}^B$ ($c_{z_4 z_4, P_joint}^B$) are the linear compliance coefficients of the spherical (prismatic) joint along the y_4 and z_4 axes; $c_{y_4 z_4, S_joint}^B$ is the coupled compliance coefficient of the spherical joint between the two directions. Note that $c_{y_4 y_4, P_joint}^B$ is constant while the others are configuration dependent and can be further formulated as

$$c_{y_4, S_joint}^B = \hat{\mathbf{y}}^T \left(\sum_{j=1}^3 (\mathbf{R}_{4j} \mathbf{C}_{j, R_joint}^B \mathbf{R}_{4j}^T) \right) \hat{\mathbf{y}} \quad (29)$$

$$c_{z_4, S_joint}^B = \hat{\mathbf{z}}^T \left(\sum_{j=1}^3 (\mathbf{R}_{4j} \mathbf{C}_{j, R_joint}^B \mathbf{R}_{4j}^T) \right) \hat{\mathbf{z}} \quad (30)$$

$$c_{y_4 z_4, S_joint}^B = \hat{\mathbf{y}}^T \left(\sum_{j=1}^3 (\mathbf{R}_{4j} \mathbf{C}_{j, R_joint}^B \mathbf{R}_{4j}^T) \right) \hat{\mathbf{z}} \quad (31)$$

$$c_{z_4 z_4, P_joint}^B = \frac{q - L_0}{EA} + c_{nut} + c_{bearing} + \left(\frac{l_b}{2\pi} \right)^2 c_{motor} \quad (32)$$

where

$$\mathbf{C}_{j, R_joint}^B = \begin{pmatrix} c_{x_j x_j, R_joint}^B & c_{y_j x_j, R_joint}^B & c_{z_j x_j, R_joint}^B \\ c_{x_j y_j, R_joint}^B & c_{y_j y_j, R_joint}^B & c_{z_j y_j, R_joint}^B \\ c_{x_j z_j, R_joint}^B & c_{y_j z_j, R_joint}^B & c_{z_j z_j, R_joint}^B \end{pmatrix}, \quad \hat{\mathbf{y}} = (0 \ 1 \ 0)^T, \quad \hat{\mathbf{z}} = (0 \ 0 \ 1)^T$$

sym

$c_{x_j x_j, R_joint}^B$, $c_{y_j y_j, R_joint}^B$ and $c_{z_j z_j, R_joint}^B$ are the linear compliance coefficients of the j th ($j=1,2,3$) revolute joint within the spherical joint along the x_j , y_j , z_j axes, respectively; while $c_{x_j y_j, R_joint}^B$ (or $c_{y_j x_j, R_joint}^B$), $c_{x_j z_j, R_joint}^B$ (or $c_{z_j x_j, R_joint}^B$) and $c_{y_j z_j, R_joint}^B$ (or $c_{z_j y_j, R_joint}^B$) are the coupled linear compliance coefficients between the three orthogonal

axes; EA and l_p are the tensile modulus and lead of the lead screw, respectively; $c_{bearing}$ and c_{nut} are the compliance coefficients of the nut and support bearing; c_{motor} is the equivalent torsional compliance of the motor; and L_0 denotes the distance between the R joint and the support bearing.

3.5 Formulation of ρ_{ta}'' and ρ_{tc}''

Continuing the approach used for the compliance components associated with the two sub-assemblies discussed in Section 3.4, $\rho_{ta,i}''$ and $\rho_{tc,i}''$ given in Eqs.(16) and (17) can be expressed as

$$\rho_{ta,i}'' = \sum_{k=1}^2 \delta_{z_{4,i},k}''^B, \quad \rho_{tc,i}'' = \sum_{k=1}^2 \delta_{y_{4,i},k}''^B \quad (33)$$

where $\delta_{y_{4,i},k}''^B$ ($\delta_{z_{4,i},k}''^B$) is the deflection at B_i along the $y_{4,i}$ ($z_{4,i}$) axis caused by the compliance of the k th sub-assembly under the action of its own gravity. Note that, in practice, $\delta_{y_{4,i},2}''^B$ and $\rho_{ta,i}''$ will be much smaller in value than $\delta_{y_{4,i},1}''^B$ and $\rho_{tc,i}''$ and can be neglected. Therefore, we take into account only the deflection $\delta_{y_{4,i},1}''^B$ which depends mainly upon two factors, i.e.,

$$\begin{aligned} \delta_{y_{4,i},1}''^B &= \delta_{y_{4,i},R_joint}''^B + \delta_{y_{4,i},L_body}''^B \\ \delta_{y_{4,i},R_joint}''^B &= -m_L g \left(c_{y_5,R_joint}^A + l_L q_i c_{\alpha_5,R_joint}^A \right) s_{5,i}^T \hat{y} \end{aligned} \quad (34)$$

where $\delta_{y_{4,i},R_joint}''^B$ is the deflection at B_i along the $y_{4,i}$ axis caused by the compliance of the revolute joint under the action of the gravity of the limb-body assembly; $\delta_{y_{4,i},L_body}''^B$ is that caused by the compliance of the limb-body assembly under the action of its own gravity, which can be modeled as a function of q_i by an interpolation technique using data obtained from finite element analysis.

4. An Example

Equipped with the compliance model developed in Section 3, we take the 5-DOF hybrid manipulator shown in Fig. 1 as an example to investigate the payload and gravity of the platform and limb-body assemblies on the pose accuracy of the end-effector. As shown in Fig.2, the task workspace W_t of the manipulator is a cylinder of radius R and height h with a distance H from the x - y plane to its inner (right-hand) bound and an offset f along the $-y$ axis. Partially referencing the current design of the Exechon 700 robot [7], the dimensions, component compliance coefficients, masses and center of mass locations of the relevant components are given in Tables 1-5. All the data are extracted from the 3-D model and evaluated by finite element analysis and/or product specifications.

Table 1 Dimensions and workspace of the 3-SPR parallel mechanism

a_1 (mm)	a_2 (mm)	b_1 (mm)	b_2 (mm)	d (mm)	e (mm)	φ (°)	H (mm)	R (mm)	h (mm)	f (mm)
240	220	570	550	20	477	12	1300	750	240	200

Table 2 Compliance coefficients of the first sub-assembly evaluated in the body fixed frames (units: $\times 10^{-3}$)

$c_{y_4 y_4, L_body}^B$ ($\mu m/N$)	$c_{z_4 z_4, L_body}^B$ ($\mu m/N$)	$c_{y_4 z_4, L_body}^B$ ($\mu m/N$)	$c_{y_5 y_5, R_joint}^A$ ($\mu m/N$)	$c_{z_5 z_5, R_joint}^A$ ($\mu m/N$)	$c_{x_5 \alpha_5, R_joint}^A$ (rad/Nm)
4.431~7.592	1.6	0.021~0.024	0.862	0.508	2.816×10^{-5}

Table 3 Compliance coefficients of the S joint evaluated in the body fixed frames (units: $10^{-3} \times \mu m/N$)

$C_{x_1 y_1, R_joint}^B$	$C_{y_1 y_1, R_joint}^B$	$C_{z_1 z_1, R_joint}^B$	$C_{x_2 x_2, R_joint}^B$	$C_{y_2 y_2, R_joint}^B$	$C_{z_2 z_2, R_joint}^B$	$C_{x_3 x_3, R_joint}^B$	$C_{y_3 y_3, R_joint}^B$	$C_{z_3 z_3, R_joint}^B$
3.045	2.678	0.711	0.897	0.470	0.426	0.483	1.039	2.146

Table 4 Coupled compliance coefficients of the S joint evaluated in the body fixed frames (units: $10^{-3} \times \mu\text{m} / \text{N}$)

$C_{x_1 y_1, R_joint}^B$	$C_{x_1 z_1, R_joint}^B$	$C_{y_1 z_1, R_joint}^B$	$C_{x_2 y_2, R_joint}^B$	$C_{x_2 z_2, R_joint}^B$	$C_{y_2 z_2, R_joint}^B$	$C_{x_3 y_3, R_joint}^B$	$C_{x_3 z_3, R_joint}^B$	$C_{y_3 z_3, R_joint}^B$
0.0615	0.0472	0.0251	0.0524	0.0253	0.0367	0.0147	0.0738	0.0154

Table 5 Parameters of the lead-screw and motor

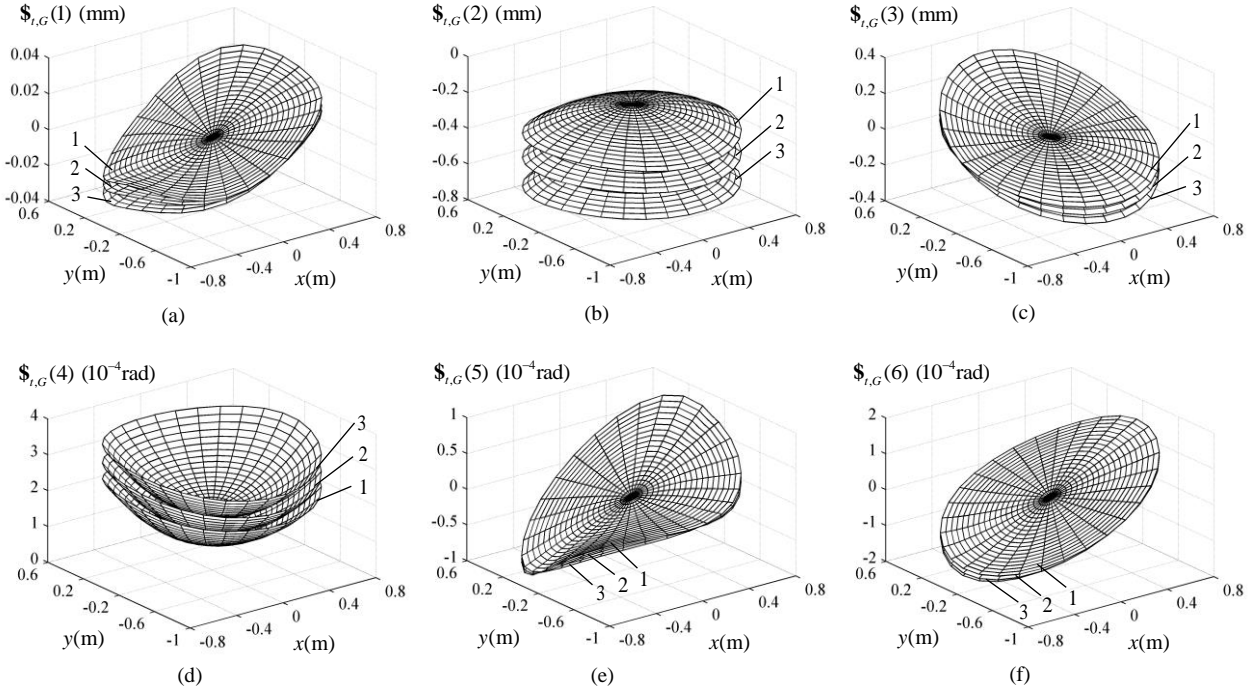
$c_{bearing}$ (nm / N)	c_{nut} (nm / N)	L_0 (mm)	EA (MN)	l_b (mm)	c_{motor} (rad / Nm)	$C_{y_4 y_4, P_joint}^B$
1.191	0.7	480	161	12	3×10^{-6}	0.062

Table 6 Masses and their locations of the platform and limb-body assembly

$r_{G0,x}$ (mm)	$r_{G0,y}$ (mm)	$r_{G0,z}$ (mm)	m_0 (kg)	m_L (kg)	l_L (mm)	t (mm)
-2.51	-6.66	181.26	144.5	174	935.1	72.43

$$\mathbf{r}_{G0} = \begin{pmatrix} r_{G0,x} & r_{G0,y} & r_{G0,z} \end{pmatrix}^T$$

For convenience, let $\$_{i,G}(i)$ ($i=1,2,\dots,6$) be the i th element of $\$_{i,G}$ sequentially representing the linear (angular) deflection along (about) the three orthogonal axes of $\{R\}$. For example, $\$_{i,G}(1)$ ($\$_{i,G}(4)$) represents the translational (rotational) deflection along (about) the x axis. Fig.9 plots how these elements vary within the workspace, showing that $\$_{i,G}(2)$, $\$_{i,G}(3)$, and $\$_{i,G}(4)$ are symmetrically distributed with respect to the y - O - z plane, with $\$_{i,G}(2)$ and $\$_{i,G}(4)$ being almost axially symmetric. However, $\$_{i,G}(1)$, $\$_{i,G}(5)$, and $\$_{i,G}(6)$ are anti-symmetrically distributed with respect to the y - O - z plane. It also shows that $\$_{i,G}(2)$, $\$_{i,G}(3)$ and $\$_{i,G}(4)$ are the key factors dominating the linear and angular deflections.

Fig.9 The distribution of $\$_{i,G}$ within W_i , 1: $z = H$, 2: $z = H + 0.5h$, 3: $z = H + h$

In order to compare the deflection $\$_{i,G}(i)$ caused by gravity with that $\$_{i,E}(i)$ caused by external force, according to [16], give the special applied forces as $F_x = 215\text{N}$, $F_y = -10\text{N}$, $F_z = -25\text{N}$, $M_x = 1\text{Nm}$, $M_y = 21.5\text{Nm}$, which are caused by groove milling. Table 6 shows the result when the manipulator stays at configuration(1) (i.e $\mathbf{r} = (0 \quad -f \quad H + 0.5h)$). It shows that the deflection caused by gravity is not negligible since it is even bigger than the deflection caused by the cutting force, especially for the translational deflection along the y axis and the rotational deflection about the x axis.

Table 7 The deflection respectively caused by the cutting forces and gravity at configuration(1)

i	1(mm)	2(mm)	3(mm)	4(10^{-4} rad)	5(10^{-4} rad)	6(10^{-4} rad)
$\$_{t,E}(i)$	0.0162	-0.002	-1.6698×10^{-4}	0.0138	0.1163	0.0082
$\$_{t,G}(i)$	7.97×10^{-6}	-0.328	1.72×10^{-4}	1.37	0.0015	0.0020

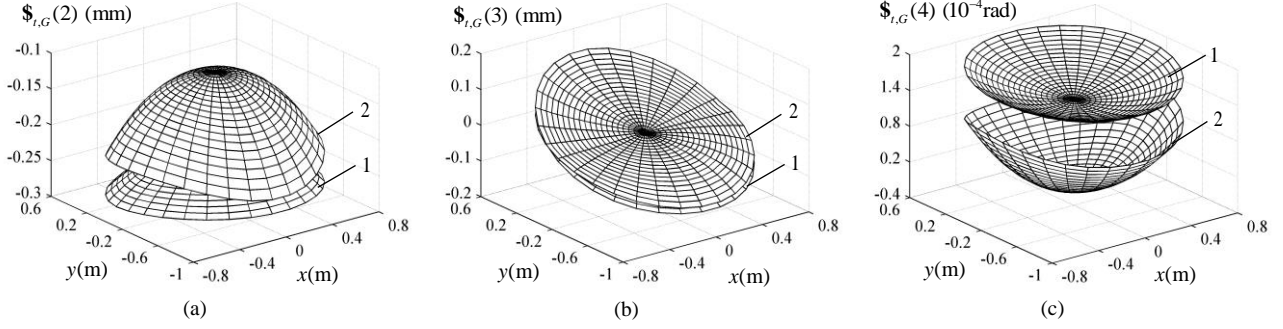
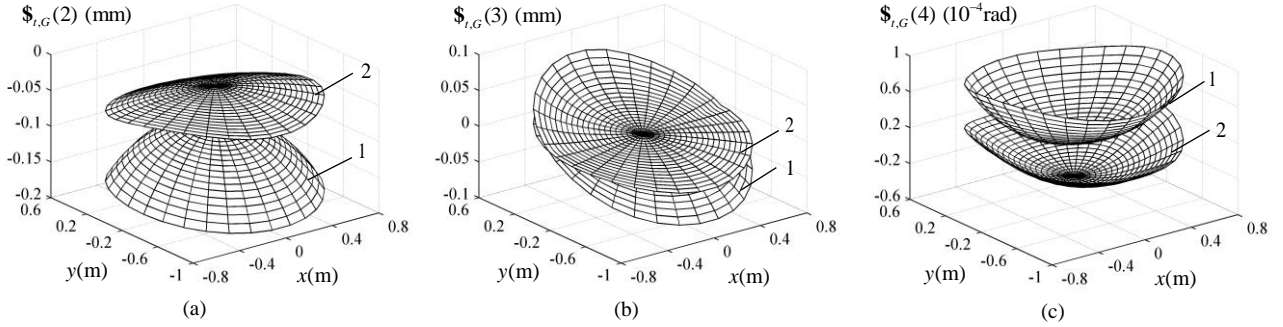

 Fig.10 The distribution of $\$_{t,G_p}$ and $\$_{t,G_L}$ at $z = H + 0.5h$, 1: $\$_{t,G} = \$_{t,G_p}$, 2: $\$_{t,G} = \$_{t,G_L}$

 Fig.11 The distribution of $\$'_{t,G_L}$ and $\$''_{t,G_L}$ at $z = H + 0.5h$, 1: $\$_{t,G} = \$'_{t,G_L}$, 2: $\$_{t,G} = \$''_{t,G_L}$

Fig.10 shows the distributions of $\$_{t,G}(2)$, $\$_{t,G}(3)$ and $\$_{t,G}(4)$ in the middle layer of W_t due to the gravity of the platform and limb-body assemblies. Clearly, the three elements $\$_{t,G}(2)$, $\$_{t,G}(3)$ and $\$_{t,G}(4)$ are all heavily affected by the gravity of the platform. A lightweight design is, therefore, absolutely necessary for reducing the platform deflection.

Fig.11 shows the distributions of $\$_{t,G}(2)$, $\$_{t,G}(3)$ and $\$_{t,G}(4)$ in the middle layer of W_t caused separately by the gravity of the limb body assemblies that is transmitted to the platform and by the compliances of the limbs under the actions of their own distributed gravity. In the three $\$_{t,G}(2)$, $\$_{t,G}(3)$ and $\$_{t,G}(4)$ the effects of the distributed gravity are smaller but also important compared with those caused by the lumped gravity transmitted to the platform. In fact, Between them, which one is bigger or smaller is depended on the structure of the limb body. As a result, their distribution, in return, can provide guidance for improving the design. For example, the results obtained by Fig.11 may show that there is room for improvement through reducing the weight of the limb body assembly.

In order to identify the weak links within the limb body assembly, the following global indices are defined

$$\bar{\$}_{t,G}(2) = \frac{\int_{W_t} \$_{t,G}(2) dV}{V}, \quad \bar{\$}_{t,G}(3) = \frac{\int_{W_t} \$_{t,G}(3) dV}{V}, \quad \bar{\$}_{t,G}(4) = \frac{\int_{W_t} \$_{t,G}(4) dV}{V} \quad (33)$$

where V denotes the volume of W_t , $\bar{\$}_{t,G}(2)$, $\bar{\$}_{t,G}(3)$ and $\bar{\$}_{t,G}(4)$ represent the mean values of $\$_{t,G}(2)$, $\$_{t,G}(3)$ and $\$_{t,G}(4)$ throughout W_t . As seen from Fig.12, the compliances of the spherical joint have the major effect on the three $\bar{\$}_{t,G}(2)$, $\bar{\$}_{t,G}(3)$ and $\bar{\$}_{t,G}(4)$, with sequentially smaller influences from the active prismatic joint (including the lead screw assembly), the limb body, and the revolute joints. These observations indicate that: (1) the rigidity of the spherical joint should be improved for resisting against gravity of the platform and limbs; (2) the weight of the limb-body assembly at the same time should be reduced without losing too much its bending rigidity. Therefore, to

ensure a light weight yet rigid design of the overall system (given a maximum allowable deflection of the platform within the entire task workspace), two of the open issues that remain to be investigated are: how to achieve compact yet rigid design of these joints; and how to balance the weights and rigidities of all the movable components. These issues must, however, be addressed in a separate paper.

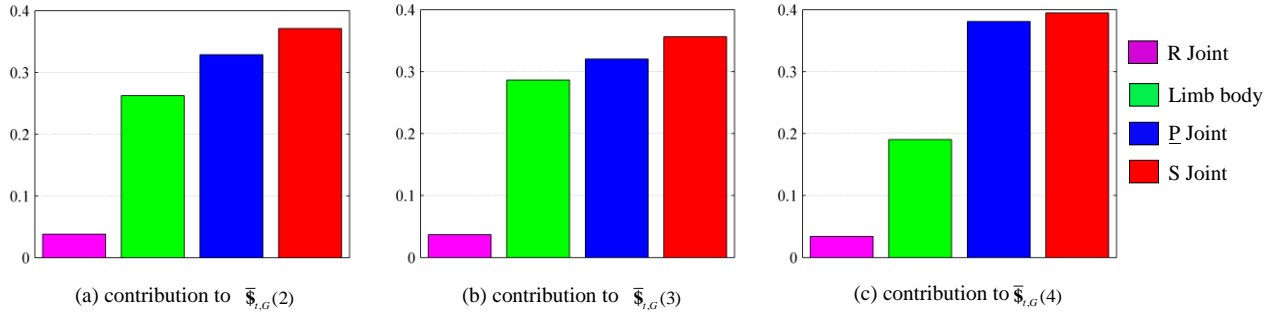


Fig.12 Contributions of the main component compliances to global deflection

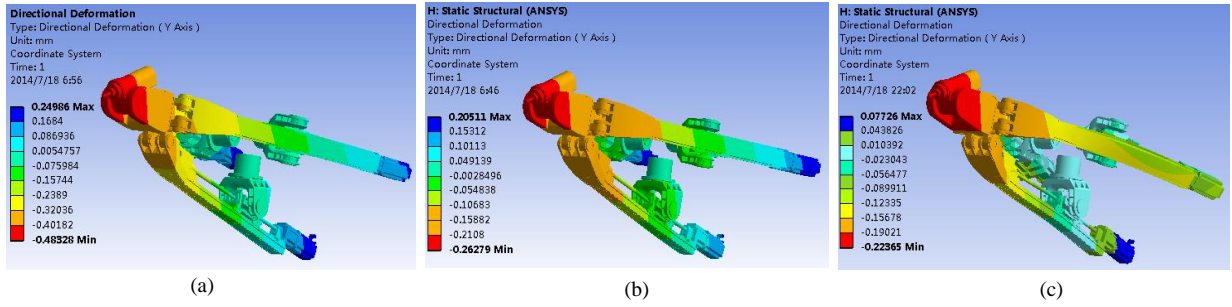


Fig. 13 Deflections along the y axis arising from gravity of (a) the platform and limb-body assemblies (b) the platform (c) the limb-body assemblies at configuration(2)

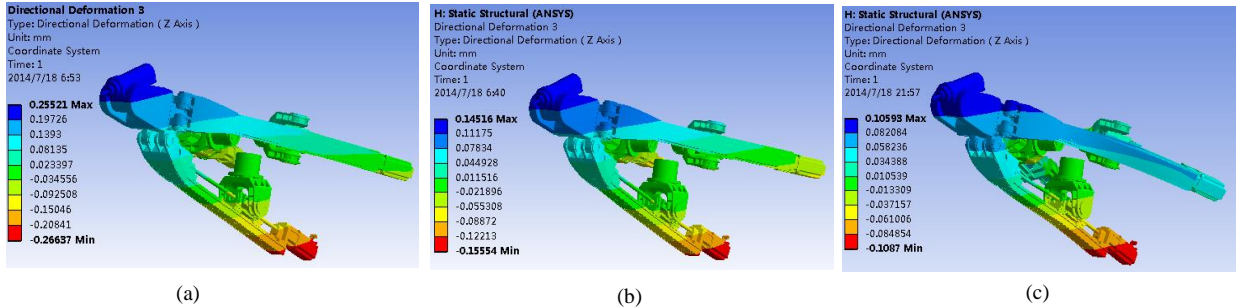


Fig. 14 Deflections along the z axis arising from gravity of (a) the platform and limb-body assemblies (b) the platform (c) the limb-body assemblies at configuration(2)

Table 8 Results obtained by the semi-analytic method and by FEA (units: mm)

		$\delta_{t,G}(2)$	$\delta_{t,Gp}(2)$	$\delta_{t,Gl}(2)$	$\delta_{t,G}(3)$	$\delta_{t,Gp}(3)$	$\delta_{t,Gl}(3)$
Configuration (1)	Semi-Analytic	-0.328	-0.211	-0.117	-0.00185	0.00041	-0.00226
	FEA	-0.305	-0.196	-0.112	-0.0017	0.00038	-0.0021
	Errors	7.5%	8.1%	4.5%	8.8%	7.9%	7.6%
Configuration (2)	Semi-Analytic	-0.538	-0.288	-0.250	0.257	0.149	0.108
	FEA	-0.483	-0.262	-0.223	0.255	0.145	0.105
	Errors	11.3%	9.9%	12.1%	0.78%	2.8%	2.9%

In order to validate the results obtained by the semi-analytical approach, an FEA deflection analysis is implemented by ANSYS®, at two typical configurations; i.e. Configuration (1) with $\mathbf{r} = (0 \quad -f \quad H+0.5h)$ and Configuration (2) with $\mathbf{r} = (R \quad -f \quad H+0.5h)$. It should be pointed out that in the FE modelling of the manipulator the base and the platform (including the 2-DOF rotating head) are treated as rigid bodies in order to match the boundary conditions assumed in the semi-analytic analysis. Meanwhile, the bushing joint defined in ANSYS® is used to model the rigidities of either a revolute or a prismatic joint along/about three orthogonal axes in its own local body-fixed frame. Please note

that the compliance coefficients of a joint are set in such a way that they are identical to those used in the semi-analytic analysis. Figs. 13 and 14 show the deflections of the manipulator in the direction of the y and the z axes arising from gravity of the platform, the limb-body assemblies, and the both, respectively; and Table 7 summarizes the simulated deflections of point P in the corresponding directions. It can be seen that the results obtained by the semi-analytic approach match very well with those evaluated by FEA for the three cases at different configurations, thus convincing the validity of the proposed semi-analytic approach.

5. Conclusions

By taking gravity into account, we propose a semi-analytic approach for compliance analysis, applied to a 3-SPR parallel mechanism. The following conclusions are drawn.

- (1) Kinetostatic analysis confirms the benefits of treating contributory components in groups related to different functional aspects of the machine. The resultant externally applied wrench imposed upon the platform contains two components, one associated with the payload and gravity of the platform, the other with the lumped gravity of the limb body assemblies. The resultant deflection twist of the platform also contains two components, one associated with the joint deflections arising from the resultant externally applied wrench, and the other from the limb body assemblies under the action of their distributed gravity.
- (2) The semi-analytical approach proposed for formulating and computing the actuated and constrained components compliance and the joint deflections due to the distributed gravity of the limb body assemblies allows the deflection of the platform within the entire task workspace to be evaluated in an efficient and accurate manner.
- (3) For the considered 5-DOF hybrid manipulator, the gravity of moving components, especially the platform (including the 2-D rotating head) is a key factor strongly affecting the pose accuracy of the end-effector, leading to an issue in need of considerable further investigation for achieving a light weight yet rigid design of the limb-body assemblies and the 2-D rotating head. This, however, deserves to be addressed in separate papers.

Acknowledgements

This research work is partially supported by the National Natural Science Foundation of China (NSFC) under grant 51135008, the Ph.D. Programs Foundation of Ministry of Education of China under grant 20110032130006, and the Alexander von Humboldt (AvH) Foundation of Germany.

References

- [1] L. W. Tsai, *Robot Analysis: The Mechanics of Serial and Parallel Manipulators*, Wiley, New York, 1999.
- [2] T. Huang, M. Li, M. L. Wu, J. P. Mei, X. M. Zhao, S. J. Hu, "The criteria for conceptual design of reconfigurable PKM modules—theory and application," *Chin. J. Mech. Eng.*, 41(8) (2005) 36–41.
- [3] J. L. Olazagoitia, S. Wyatt, New PKM Tricept T9000 and its application to flexible manufacturing at aerospace industry[R]// SAE International, (2007) Paper No. 07ATC-94.
- [4] H. K. Tonshoff, H. Grendel, R. Kaak, "Structure and characteristics of the hybrid manipulator George V, Parallel Kinematic Machines, C. R. Boer, L. Molinari-Tosatti, and K. S. Smith, eds., Springer-Verlag, London, (1999) 365–376.
- [5] T. Huang, M. Li, X. M. Zhao, et al. Conceptual design and dimensional synthesis of 3-DOF module of the TriVariant a novel 5-DOF reconfigurable hybrid robot, *IEEE Transactions on Robotics*, 21(3) (2005) 449–456
- [6] C. Zielinski, K. Mianowski, K. Nazarczuk, W. Szykiewicz, A prototype robot for polishing and milling large objects, *Ind. Robot*, 30(1) (2003) 67–76.
- [7] Z. M. Bi, Kinetostatic modeling of Exechon parallel kinematic machine for stiffness analysis, *The International Journal of Advanced Manufacturing Technology*, (2013) 1–11.
- [8] G. Piras, W. L. Cleghorn, J. K. Mills, Dynamic finite-element analysis of a planar high-speed, high-precision parallel manipulator with flexible links, *Mechanism and Machine Theory* 40(7) (2005) 849–862.
- [9] T. Bonnemaïn, H. Chanal, B. C. Bouzgarrou, P. Ray, Stiffness computation and identification of parallel kinematic machine tools, *Journal of Manufacturing Science and Engineering* 131(4) (2009) 041013-7.
- [10] C. M. Gosselin, Stiffness mapping for parallel manipulators, *IEEE Trans. on Robotics and Automation* 6(3) (1990) 377–382.
- [11] D. Zhang, C. M. Gosselin, Kinetostatic modelling of N-DOF parallel mechanisms with a passive constraining leg and prismatic actuators, *ASME Journal of Mechanical Design* 123(9) (2001) 375–381.
- [12] C. M. Gosselin, D. Zhang, Stiffness analysis of parallel mechanisms using a lumped model, *International Journal of Robotics and Automation* 17(1) (2002) 17–27.
- [13] D. Zhang, Z. M. Bi, B. Z. Li, Design and kinetostatic analysis of a new parallel manipulator, *Robotics and Computer-Integrated Manufacturing* 25(4-5) (2009) 782–791.
- [14] A. Pashkevich, D. Chablat, Ph. Wenger, Stiffness analysis of over-constrained parallel manipulators, *Mechanism and Machine Theory* 44(5) (2009) 966–982.
- [15] A. Klimchik, A. Pashkevich, S. Caro, D. Chablat, Stiffness matrix of manipulators with passive joints: computational aspects, *Robotics, IEEE Transactions on*, 28(4), (2012) 955–958.
- [16] A. Klimchik, D. Chablat, A. Pashkevich. Stiffness modeling for perfect and non-perfect parallel manipulators under internal and external loadings[J]. *Mechanism and Machine Theory*, 79, (2014) 1–28.
- [17] Y. M. Li, Q. S. Xu, Kinematics and stiffness analysis for a general 3-PRS spatial parallel mechanism, *Proceedings of IFToMM Symposium on Robot Design and Dynamics*, Montreal, Canada, 2004.
- [18] H. S. Kim, C. R. Shin, J. H. Kyung, et al., Stiffness analysis of a low-DOF parallel manipulator including the elastic deformations of both joints and links, *Proceedings of the International Conference on Control, Automation and Systems*, Gyeonggi-Do, Korea, 2005.
- [19] J. W. Kim, K. W. Kim, H. S. Kim, J. H. Kyung, Stiffness analysis and design of a 3-DOF parallel robot with one constraining

- leg, Proceedings of the International Conference on Control, Automation and Systems, Seoul, Korea, 2007, 2288-2293.
- [20] Y. M. Li, Q. S. Xu, Stiffness analysis for a 3-PUU parallel kinematic machine, *Mechanism and Machine Theory* 43(2) (2008) 186-200.
 - [21] B. Li, H. Yu, Z. Deng, X. Yang, H. Hu, Stiffness modeling of a family of 6-DoF parallel mechanisms with three limbs based on screw theory, *Journal of mechanical science and technology*, 24(1) (2010) 373-382.
 - [22] B. Hu, Y. Lu, Solving stiffness and deformation of a 3-UPU parallel manipulator with one translation and two rotations, *Robotica*, 29(6) (2011) 815-822.
 - [23] H. T. Liu, Y. G. Li, T. Huang, et al. An approach for stiffness modelling of lower mobility parallel manipulators using the generalized jacobian. 13th World Congress in Mechanism and Machine Science, Guanajuato, México. 2011, 19-25.
 - [24] G. Cheng, P. Xu, D. Yang, et al. Stiffness analysis of a 3CPS parallel manipulator for mirror active adjusting platform in segmented telescope, *Robotics and Computer-Integrated Manufacturing*, (29) (2013) 302-311.
 - [25] D. Wang, R. Fan, W. Chen, Stiffness analysis of a hexaglide parallel loading mechanism, *Mechanism and Machine Theory*, 70, (2013) 454-473.
 - [26] Y. Li, E. Zhang, Y. Song, Z. Feng, Stiffness modeling and analysis of a novel 4-DOF PKM for manufacturing large components, *Chinese Journal of Aeronautics*, 26(6) (2013), 1577-1585.
 - [27] S. Joshi, L. W. Tsai, Jacobian analysis of limited-DOF parallel manipulators, *ASME J. Mechanical Design* 124(2) (2002) 254-258.
 - [28] T. Huang, H. T. Liu, D.G. Chetwynd, Generalized Jacobian analysis of lower mobility manipulators, *Mechanism and Machine Theory* 46(5) (2011) 831-844.
 - [29] T. S. Zhao, Y. Z. Zhao, H. Bian, N. Li, Continuous stiffness nonlinear mapping of spatial parallel mechanism. *Chinese Journal of Mechanical Engineering* 44(8) (2008) 20-25 (Chinese).
 - [30] C. Quennouelle, C. M. Gosselin, Kinemastatic modeling of compliant parallel mechanisms. *Meccanica*, 46(1) (2011) 155-169.
 - [31] C. Quennouelle, C. M. Gosselin, A general formulation for the stiffness matrix of parallel mechanisms. *arXiv preprint arXiv: 2012.1212.0950*.
 - [32] M. X. Wang, T. Huang, Kinematics analysis and dimensional synthesis of a plane symmetric 3-SPR parallel manipulator, *Chin. J. Mech. Eng.*, 49(15), 2013, 22-27.